Title: BODIPY-Based Photothermal Agents for Cancer Treatment

Authors:

Lukas Schneider,[‡1] Martina Kalt,[‡,§1,2] Samuel Koch,[1] Shanmugi Sithamparanathan,[1] Veronika Villiger,[1] Johann Mattiat,[1] Flavia Kradolfer,[1] Ekaterina Sylshkina,[1] Sandra Luber,[1] Mathias Bonmarin,[3] Caroline Maake,[2] and Bernhard Spingler[*1]

[‡] These authors contributed equally to the work.

[§] Current affiliation: EAWAG, CH-8600 Dübendorf, Switzerland

[*] To whom correspondence should be addressed. E-mail: spingler@chem.uzh.ch

Affiliations:

[1] Department of Chemistry, University of Zurich, CH-8057 Zurich, Switzerland.

[2] Institute of Anatomy, University of Zurich, CH-8057 Zurich, Switzerland.

[3] School of Engineering, Zurich University of Applied Sciences, CH-8400 Winterthur, Switzerland.

Abstract:

Here we report six novel, easily accessible BODIPY-based agents for cancer treatment. In contrast to established photodynamic therapy (PDT) agents, these BODIPY-based compounds show additional photothermal activity and their cytotoxicity is not dependent on the generation of reactive oxygen species (ROS). The agents show high photocytotoxicity upon irradiation with light and low dark toxicity in different cancer cell lines in 2D culture as well as in 3D multicellular tumour spheroids (MCTSs). The ratio of dark to light toxicity (phototoxic index, PI) of these agents reaches striking values exceeding 830'000 after irradiation with energetically low doses of light at 630 nm. The oxygen-dependent mechanism of action (MOA) of established photosensitizers (PSs) hampers effective clinical deployment of these agents. Under hypoxic conditions (0.2% O_2), which are known to limit the efficiency of conventional PSs in solid tumours, a PI of 360'000 was observed, indicating an oxygen-independent photothermal MOA. Both PI values are the highest reported to date. We anticipate that small molecule agents with a photothermal MOA, such as BODIPY-based compounds, may overcome this barrier and provide a new avenue to cancer therapy.

Keywords:

Medicinal Chemistry, Photodynamic Therapy, Photothermal Therapy, Phototherapy, Cancer

Introduction:

In the last couple of decades, photodynamic therapy (PDT) has become a widely used therapeutic method for the treatment of a variety of premalignant and malignant diseases.[1-3]

PDT conventionally involves the application of a photosensitizer (PS) that is activated by light in the tissue to be treated. This method has many potential applications due to the advantages it presents as a non- or minimally invasive therapeutic. PDT does not exhibit cumulative toxicity and its activation can be controlled both spatially and temporally. The adjustable light used, as well as the short diffusion radius of the emerging reactive oxygen species (ROS), minimize the damage to surrounding healthy tissue.[4-5]

The mechanism of action (MOA) consists of the PS-mediated generation of ROS from its first excited triplet state.[6] The generated ROS involves singlet oxygen ($^1O_2$) via the type II mechanism, or radical species such as hydroxyl radicals ($OH^\bullet$) and superoxide anions ($O_2^{\bullet-}$) via the type I mechanism.[7] Both mechanisms depend on molecular oxygen ($^3O_2$) in the tissue, leading to reported clinical resistance under hypoxia. This MOA is a major drawback as solid tumours are invariably less well-oxygenated than non-malignant tissue.[8-12]

Alternative MOAs to the type I and type II pathways have been reported in literature despite a lack of consensus regarding the definition of oxygen-independent mechanisms.[10, 13] A modified type I mechanism, called type III, has been described based on an interaction between the PS in its first excited triplet state and doublet free radicals with diffusion-controlled rate constants.[14-19] Other reports of oxygen-independent mechanisms involve the generation of toxic photoproducts from upper excited triplet states,[20] photoinduced electron-transfers leading to cycloaddition reactions,[21-22] and structural changes upon excitation that allow binding to intracellular targets.[10, 18] These properties currently preclude therapeutic deployment. Additional agents for phototherapy undergoing photoredox catalysis have been reported recently.[23-24]

Furthermore, phototherapeutic treatment methods have emerged based on photothermal therapy (PTT). PTT applies functional biomedical and bioactive nanomaterials activated by light in the near-infrared (NIR) range to eliminate tumour cells via the generation of heat upon irradiation.[25-27] Despite the many advantages of PTT, drawbacks concerning biocompatibility, biodegradation, long-term toxicity, and threats of these nanomaterials to the environment remain unresolved.[25] Small molecules rather than nanomaterials have been employed for PTT, however all the previous approaches required a nanoprecipitation step, again precluding straightforward use in a biological context.[28-30]

Here, we report six novel metal-free BODIPY-based (boron-dipyrromethene) agents that undergo an oxygen-independent photothermal MOA upon excitation with small doses of light in the visible range. The compounds are easily accessible and have phototoxic indices (PIs), the ratio of dark to light toxicity,[31-32] of over 830'000 in cancer cells under normoxic conditions and over 360'000 under hypoxic conditions (0.2% O_2). BODIPY-based compounds have favourable properties, being easily accessible small molecules that are excitable with tissue-penetrating red light at 630 nm. In contrast to conventional PTT systems, they can be applied in solution and do not require the nanoprecipitation step prior to application. We anticipate that their toxicity to cancer cells through local light-to-heat conversion might help to overcome the enormous drawback of hypoxia resistance in PDT as well as the toxicity issues of nanomaterials in PTT.

Results:

Characterization:

All compounds are based on an asymmetric BODIPY-based structure[33] with an extended π-system and varying bathochromically-shifting moieties. BODIPYs are known for their high chemical stability and molar extinction coefficients, and their photophysical properties as well

as their solubility can be fine-tuned by countless possibilities of synthetic functionalization.[34] Therefore, they are promising candidates for light-induced cancer therapy. Compounds **1a**, **2a,** and **3a** were synthesized as described in the supporting information (**S1 – S5)** and compounds **1b**, **2b,** and **3b** were obtained after mono-iodination of compounds **1a**, **2a**, and **3a**, respectively. Compounds **1b**, **2b,** and **3b** contain an additional iodine atom to induce a heavy-atom effect and higher triplet state quantum yields[35-36] (**Fig. 1a**). All compounds were characterized as described in the supporting information (**S1 – S5)** by spectroscopic and analytical data including UV-Vis, fluorescence emission, IR, NMR, and mass spectroscopy, liquid chromatography, partition constant determination (**S6**, **Tab. S1)**, elemental analysis, as well as single crystal X-ray analysis (**Fig 1b**).

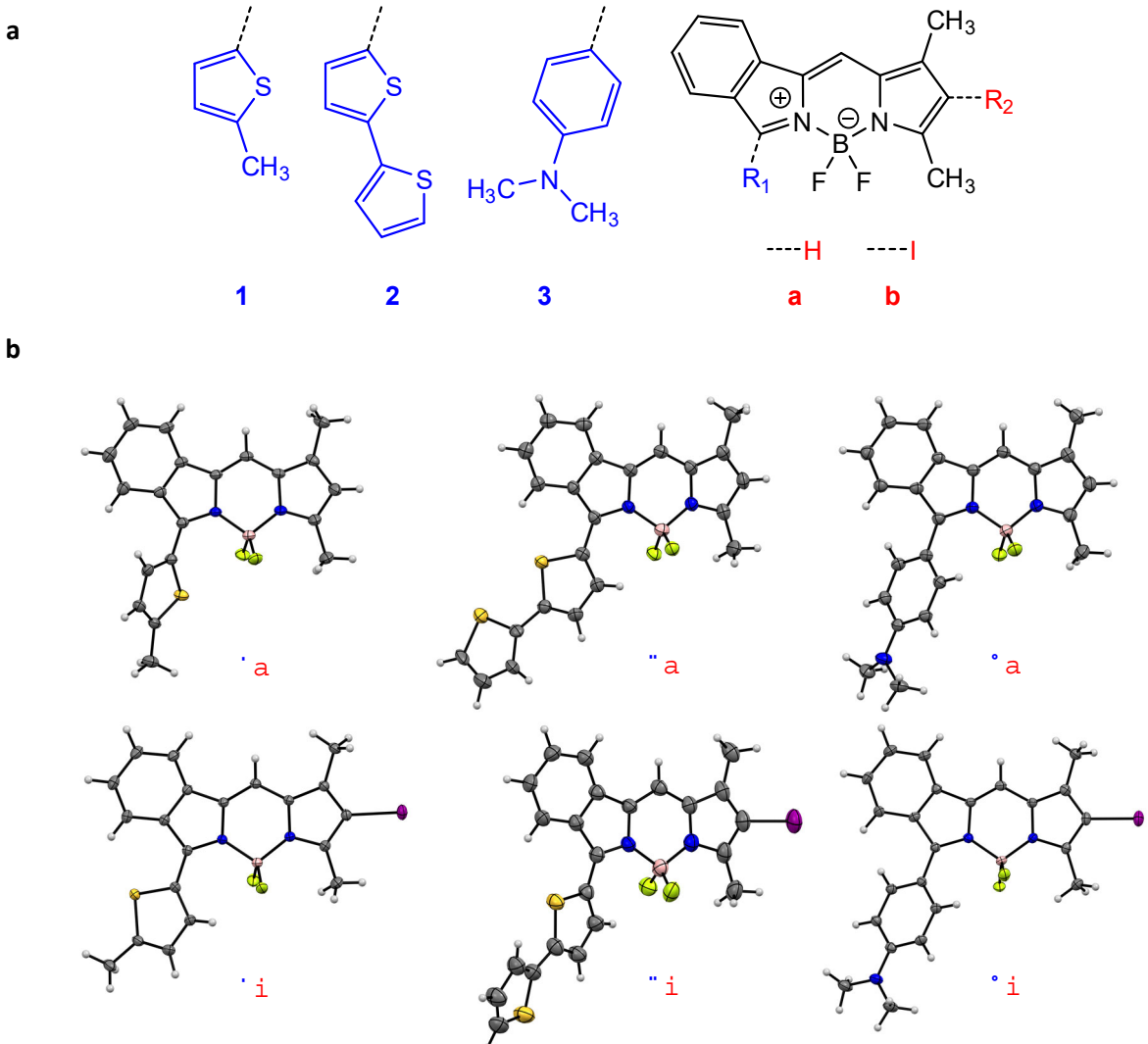

Fig. 1: **a**, Chemical structures of **1a** - **3a**, as well as **1b** - **3b**. **b**, Ellipsoidal representations of the X-ray crystal structures of **1a** - **3a**, and **1b** - **3b** (ellipsoids drawn at 50% probability). For clarity, only one out of two molecules in the asymmetric unit is shown for **1a**, the minor orientation of the disordered terminal thiophene unit has been omitted for **2a**, and one DCM co-solvent molecule has been omitted for clarity for **2b**.

Photophysical measurements were carried out for all six compounds. The singlet oxygen quantum yields (Φ_Δ) (**Tab. 1**, **Tab. S2**) of **1a**, **1b, 2a, 2b**, **3a**, and **3b** were determined by applying light at a wavelength of 630 nm (**Fig. S2**) based on a direct method[34, 37-40] as described in **S8**. Fluorescence quantum yields (Φ_F) (**Tab. 1**, **Tab. S3**) of **1a, 1b, 2a, 2b**, **3a**, and **3b** were

determined as described in **S9**. All compounds are highly fluorescent in aprotic solvents like DCM and toluene, and non-fluorescent in H_2O, and all compounds except **3a** and **3b** are highly-fluorescent in the protic solvent MeOH with Φ_F values ranging from 0.33 to 0.82, while the protic character of MeOH quenches the fluorescence emission of **3a** and **3b** to $\Phi_F \leq 0.01$. The fluorescence lifetimes (τ_F) (**Tab. 1**, **Tab. S4**) of all compounds have been determined in MeOH as described in **S10**, resulting in τ_F values in the range of 3.2 to 5.4 ns. The absorption maximum of all studied compounds is in the range between 588 and 617 nm in MeOH and the fluorescence emission maximum between 620 and 655 nm. In MeOH, DCM and toluene all compounds exhibit a rather sharp absorption maximum, while in H_2O the absorption peak is very broad with distinctly lower extinction coefficients compared to the other solvents. The addition of the iodine atom to the pyrrolic position bathochromically shifts the absorption maximum between 8 nm and 15 nm compared to the non-iodinated analogue compound. The compound pair **2a** and **2b** exhibit their absorption maximum at the longest wavelengths due to the presence of a second thiophene unit that is contributing to the photochemical system of the compounds. Non-iodinated compounds **1a**, **2a,** and **3a** do not generate $^1O_2$, while the iodine-containing derivatives **1b** and **2b** show a low Φ_Δ of 0.26 ± 0.05 and 0.15 ± 0.01, respectively, in contrast to **3b** that does not generate $^1O_2$ at all in MeOH-d_4. BODIPY-based compounds containing a *N*,*N*-dimethylaniline moiety like of **3b** are known for undergoing intramolecular charge transfers (ICTs) in the non-protonated state upon irradiation that quenches the $^1O_2$ generation.[34, 41-43] This correlates with the triplet state lifetimes (τ_T) (**Tab. 1**, **Tab. S5**) determined as described in **S11**. While a τ_T of 138.1 ± 1.7 ns was measured for **1b**, and a τ_T of 154.1 ± 1.3 ns for **2b**, no triplet state was detected for the third compound of the iodinated series, **3b**. No triplet state could be detected in the case of all non-iodinated compounds **1a**, **2a,** and **3a**, which is also in line with the observed Φ_Δ values. The ability to generate $^1O_2$ (type II mechanism) and the ability to generate hydroxyl radicals ($^\bullet$OH), superoxide anions ($O_2^{\bullet-}$) and/or other ROS (type I mechanism) (**Fig. S6**) was investigated with the corresponding chemical sensors[44] as described in **S11**. Compared to the standard methylene blue (**MB**), only small amounts of ROS were detected in the case of **1a, 1b, 2a, 2b**, **3a**, and **3b** after irradiation with light at 630 nm (**Fig. S5**) for 40 min (total applied energy = 5.0 J/cm^2). This suggests that the generation of ROS is not the primary mechanism to induce photocytotoxicity.

The first two excited singlet (S_x) and triplet (T_x) states of **1a, 1b, 2a, 2b**, **3a**, and **3b** were calculated at TDDFT level using geometry optimized structures. The BLYP exchange-correlation functional[45-46] was employed for the geometry optimizations and the TDDFT calculations. Additionally, TDDFT calculations were carried out using the B3LYP hybrid exchange-correlation functional[46-48] (**Tab. S6**). The computational methodology is described in **S13**. Visualizations of the calculated natural transition orbitals (NTOs)[49] for the first singlet states as described in **S14** provide an intuitive particle-hole picture (**Fig. S7**) after the immediate absorption. The results indicate that the long-lived first excited triplet state (T_1) is energetically accessible for all six compounds. As the calculations were carried out for optimized ground state structures the calculated energies correspond to vertical excitation energies. In order to obtain insight into the actual photochemical processes involved non-adiabatic dynamics would be required the computational cost of which goes beyond the scope of this work. Additional calculations performed using the COSMO solvation model[50] to account for solvation effects indicated comparable results (**Tab. S7**).

The photostability of all compounds was determined by measuring the photobleaching quantum yields (Φ_d) (**Tab. 1**, **Tab. S8**) as described in **S15**. Compounds **1a**, **3a,** and **3b** were photostable under the applied conditions in DMF, while **1b**, **2a,** and **2b** showed small Φ_d in comparison to zinc phthalocyanine (**ZnPc**) of (6.5 ± 0.6) × 10^{-6}, (7.8 ± 0.5) × 10^{-5}, and (6.4 ± 0.3) ×

10^{-6}, respectively.

Compound	Absorption λ_{max} (nm)	Emission λ_{max} (nm)	Φ_Δ	Φ_F	τ_F (ns)	τ_T (ns)	Φ_d
1a	590	620	0	0.82 ± 0.06	4.73 ± 0.24	-	Photostable (> 2 h)
1b	598	633	0.26 ± 0.05	0.50 ± 0.03	4.69 ± 0.01	138.1 ± 1.7	(6.5 ± 0.6) × 10^{-6}
2a	607	651	0	0.43 ± 0.01	5.40 ± 0.01	-	(7.8 ± 0.5) × 10^{-5}
2b	617	655	0.15 ± 0.01	0.33 ± 0.04	3.45 ± 0.01	154.1 ± 1.3	(6.4 ± 0.3) × 10^{-6}
3a	588	627	0	0.025 ± 0.001	4.10 ± 0.02	-	Photostable (> 2 h)
3b	597	638	0	0.010 ± 0.001	3.22 ± 0.01	-	Photostable (> 2 h)

Tab. 1: Photophysical properties of **1a**, **1b**, **2a**, **2b**, **3a,** and **3b**. UV-Vis absorption measured in MeOH; Fluorescence emission measured in MeOH; Φ_Δ measured in MeOH-d_4; Φ_F measured in MeOH; τ_F measured in MeOH; τ_T measured in MeOH; Φ_d measured in DMF. Additional UV-Vis absorption, and fluorescence emission spectra and data measured in H_2O, MeOH, DCM and toluene are reported in the Supporting Information.

Photocytotoxicity:

The photocytotoxicity of **1a, 1b, 2a, 2b**, **3a**, and **3b** (**Tab. 2**) was studied as described in **S16-S18**, the light dose dependency (**Fig. S8**) and time-dependent cellular uptake (**Fig. S9)** were determined as described in **S19-S20**. HeLa human cervical cancer cells were treated with the compounds and irradiated with light of 630 nm (**Fig. S5**) for 40 min corresponding to an energy dose of 5.0 J/cm^2. Despite the high Φ_F values, low Φ_Δ values and low levels of generated ROS, **1a, 1b, 2a, 2b**, **3a**, and **3b** showed high photocytotoxicity when exposed to this low total energy dose. The IC_{50} (half maximal inhibitory concentration) values of all iodinated compounds are in the one- or two-digit nanomolar range. As expected, they are distinctly lower than for all non-iodinated compounds. The presence of a T1 state, based on the measurable τ_T, does not correlate with the observed photocytotoxicities, and the non-iodinated compounds **1a**, **2a,** and **3a** as well as the iodinated compound **3b** show photocytotoxicity. All compounds furthermore show very low toxicity in the dark with IC_{50} values up to > 5 mM. The most interesting non-iodinated/iodinated compound pair **1a** and **1b** is non-toxic in the dark in HeLa cells (IC_{50} > 5 mM), while **1a** as the non-iodinated compound has an IC_{50} value of 0.730 ± 0.004 μM upon irradiation and **1b** as the iodinated compound has an IC_{50} value of 0.0060 ± 0.0003 μM upon irradiation. This is equal to a PI of over 830'000 for **1b**. This is, to the best of our knowledge, the highest PI value reported for any BODIPY-based compound. Photocytotoxicity determinations of **1a** and **1b** in other cell lines such as in the A2780 human ovarian cancer cell line (**Tab. S9**), and MRC-5 human fetal lung fibroblast cell line (**Tab. S10**) showed similar photochemical and phototoxic properties.

Compound	IC_{50} (irradiation, μM)	IC_{50} (dark, μM)	PI
1a	0.730 ± 0.004	> 5000	> 6800
1b	0.0060 ± 0.0003	> 5000	> 830'000
2a	0.130 ± 0.003	1250 ± 88	9600
2b	0.0350 ± 0.0009	2070 ± 269	59'000
3a	0.56 ± 0.04	1330 ± 123	2400
3b	0.032 ± 0.002	2160 ± 139	68'000

Tab. 2: IC_{50} values of **1a, 1b, 2a, 2b**, **3a**, and **3b** in the dark and upon irradiation, and the corresponding PI values. Compound **1b** is the most efficient compound with an IC_{50} value of 0.0060 ± 0.0003 μM upon light irradiation, > 5000 μM in the dark and a PI of > 830'000.

Photocytotoxicity (**Tab. S11**) and growth-inhibiting properties (**Fig. 2**) of **1b** in HeLa 3D multicellular tumour spheroids (MCTSs), which are known to simulate the conditions found in clinically treated tumors[51-52], have been determined as described in **S21-S23**. The photocytotoxicity assay with **1b** was carried out under analogous conditions to those used for determining photocytotoxicity in HeLa cell monolayers using light with a wavelength of 630 nm (**Fig. S5**) and an irradiation time of 40 min corresponding to an energy dose of 5.0 J/cm^2. IC_{50} values for **1b** in HeLa MCTSs have been determined to be 0.12 ± 0.04 μM after light exposure and > 1660 μM in the dark, resulting in a PI of > 13'800. This underlines the photocytotoxic potency of **1b** observed in the different cell lines in a simple model system with tumour-like conditions.

The growth-inhibiting properties of **1b** in HeLa MCTSs were measured before and after treatment with **1b**. MCTSs treated with **1b** and irradiated with light were compared to three control conditions: MCTSs treated with **1b** and kept in the dark, MCTSs treated with the solvent vector only and kept in the dark, and MCTSs treated with the solvent vector upon irradiation with light. All three control conditions led to linear MCTS growth during the observation window with an average MCTS size of 181% on day five compared to the initial size. MCTSs treated with **1b** and subsequent irradiation with light of 630 nm started dissolving on day three visible in the inflation of the MCTSs to 233% of the initial size followed by a steady decrease in size. This shows that **1b** is not just decreasing the growth rate of the MCTSs like cisplatin[40], but actively destroying them upon irradiation. The observed change in size of the MCTSs is shown in micrographs of single MCTSs over time (**Fig 2a**), as well as MCTS size relative to time (**Fig 2b**).

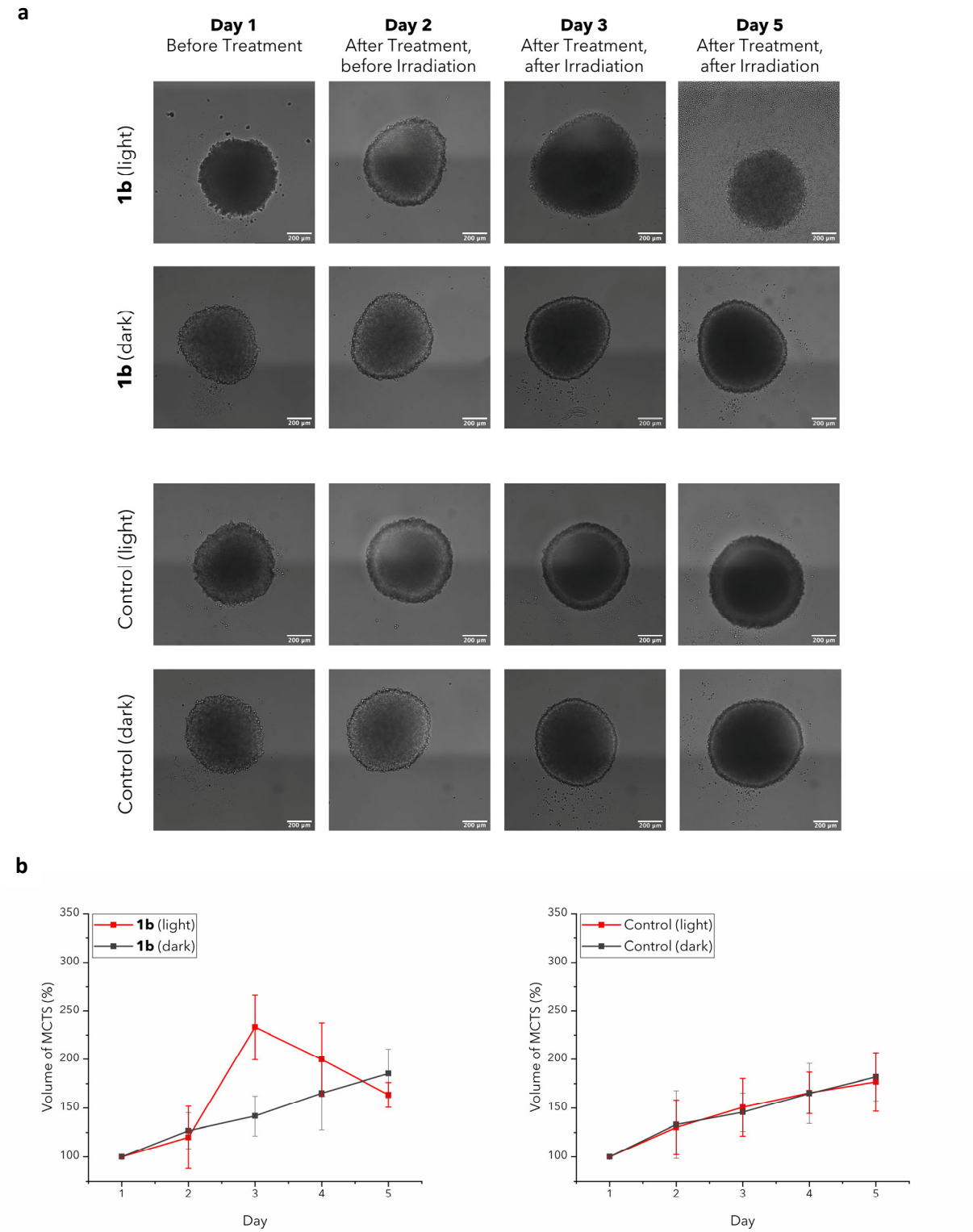

Fig. 2: **a**, Micrographs of 3D HeLa multicellular tumor spheroids (MCTSs) taken over five days (scale bars = 200 µm). **b**, Monitored growth of 3D HeLa MCTSs over five days compared to the initial size. MCTSs were treated either with **1b**, or the solvent vector (Control), and irradiated either with light of 630 nm (light), or kept in the dark (dark).

Because MCTSs also simulate tumour hypoxia and proliferation gradients to the centre[51-52], the observed effectivity in HeLa MCTSs indicated a possible efficiency under hypoxic conditions. To test this hypothesis, the photocytotoxicity determination for compounds **1a** and **1b** in

monolayer HeLa cells was repeated under hypoxic conditions (**Tab. 3**) as described in **S24**. Both **1a** and **1b** proved to be highly effective in HeLa cells under hypoxic conditions while being treated and excited analogous to conditions used to test phototoxicity in HeLa cells under normoxic conditions. IC_{50} values in the dark were, as expected, slightly lower under hypoxic conditions with values > 2500 μM for both **1a** and **1b**. While the IC_{50} value upon excitation with light of the non-iodinated compound **1a** increased to 1.87 ± 0.08 μM, the IC_{50} value of the iodinated compound **1b** remained virtually unchanged with a value of 0.0069 ± 0.0003 μM, showing that **1b** is not only highly photocytotoxic under normoxic conditions, but also under hypoxic conditions as prevalent in the majority of solid tumours[9, 53] that can lead to hypoxic drug resistance[8] especially in the case of PDT agents.[11]

Compound	IC_{50} (irradiation, μM)	IC_{50} (dark, μM)	PI
1a	1.87 ± 0.08	> 2500	> 1300
1b	0.0069 ± 0.0003	> 2500	> 360'000

Tab. 3. The photocytotoxicities and dark toxicities as well as the PIs of **1a** and **1b** in HeLa cells under hypoxic conditions (0.2% O_2, 630 nm, 5.0 J/cm^2).

Mechanism of Action:

In order to determine the cellular uptake pathway of compound **1b**, we inhibited specific uptake pathways in HeLa cells as described in **S25**. Different uptake pathways were blocked by preincubation with a cationic transporter, metabolic, and endocytotic inhibitors (**Fig. S10**).[51, 54-56] None of the blocked pathways showed an impact on the uptake efficiency of **1b**. Compared to the standard setting the uptake of **1b** is 26% lower at low temperature (4 °C). This indicates that **1b** is primarily taken up by passive diffusion. Intracellular ROS levels upon irradiation after exposure to **1b** were measured as described in **S26**. Compared to **MB** only a minor fraction of the cells tested were ROS-positive after the application of **1b** and subsequent irradiation (**Fig. S11**). This is in line with the observation of low levels of different kinds of ROS generated by **1b** in solution (**Fig. S6**). Together with the observed high photocytotoxicity under hypoxic conditions, these low ROS levels argue that an oxygen-independent MOA is the major cytotoxic pathway. Micrographs visualizing generated intracellular ROS (**Fig. S12**) were taken as described in **S27** and the results are in line with the intracellularly measured ROS levels.

Intracellular localization of **1a** and **1b** was investigated in HeLa cells (**Fig. 3**, **Fig. S13**) with different dyes for cell organelle staining as described in **S28**. Both **1a** and **1b** are observable as distinct spherical fluorescent spots and seem to behave similarly after being taken up in the cell. Neither compound co-localized with markers for the nucleus, the mitochondria, the Golgi apparatus, the endoplasmic reticulum, lysosomes or peroxisomes. This indicates that both **1a** and **1b** form local clusters in the cytosol of HeLa cells without specific accumulation in any of the tested cell organelles.

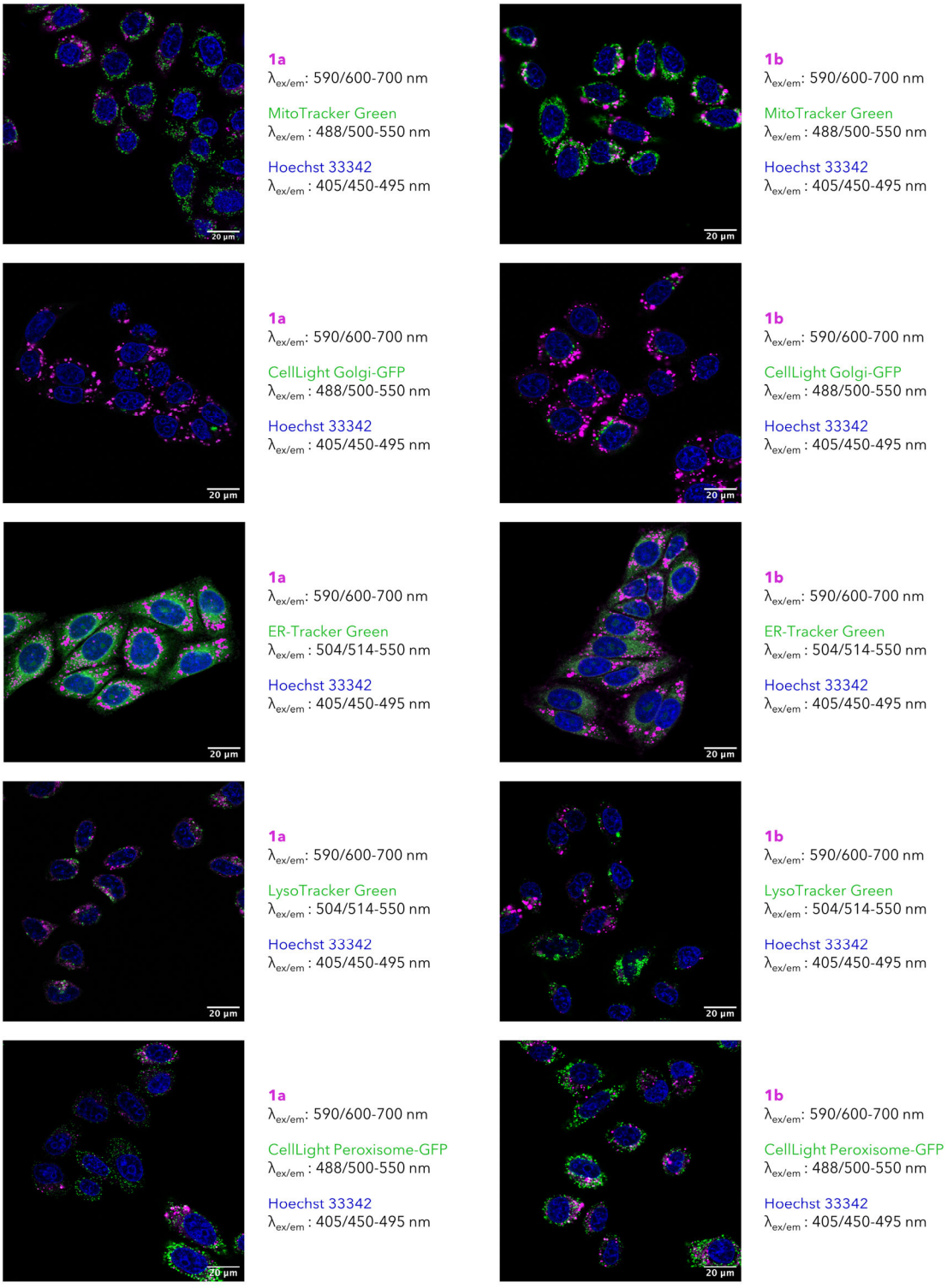

Fig. 3: Merged intracellular localization images of **1a** and **1b** in HeLa cells visualised together with the nucleus (Hoechst 33342) and mitochondria (MitoTracker Green FM), Golgi apparatus (CellLight Golgi-GFP, BacMam 2.0), endoplasmic reticulum (ER-Tracker Green), lysosomes (LysoTracker Green DND-26), or peroxisomes (CellLight Peroxisome-GFP, BacMam 2.0). Images of individual stains are reported in **Fig. S13**. No co-localization with any of the tested organelles is observable for **1a** or **1b**.

Next, we tested the ability of **1b** to disrupt the mitochondrial membrane potential (MMP) in

HeLa cells as described in **S29**. Disruption of the MMP indicates an effect on the mitochondrial electron transfer chain and a failure of mitochondrial function, and is associated with an apoptotic or necrotic cell death mechanism.[57-58] The MMP of HeLa cells was not disrupted after the application of **1b** in the concentration range 0.5 nM – 0.5 μM in the dark, while a clear disruption is visible for **1b** upon application and subsequent irradiation from an applied concentration of 5.0 nM onwards (**Fig. S14**). This concentration is in line with the observed IC_{50} value of **1b** in HeLa cells (**Tab. 2).** Visualization of MMP disruption by **1b** (**Fig. S15**) was carried out with different concentrations of **1b** in the dark, and upon irradiation as described in **S30**. The results were consistent with the MMP disruption experiments.

To investigate the cell death pathway induced by **1b** upon irradiation further, an annexin V/propidium iodide assay in HeLa cells (**Fig. S16**) was applied as described in **S31**. This assay shows through changes in the plasma membrane integrity/permeability if cells are viable, apoptotic, or necrotic.[59-60] The observed staining of HeLa cells with the isothiocyanate–annexin V conjugate is in line with the results obtained in the MMP disruption experiment (**Fig. S14**). The cells additionally showed a fluorescent signal upon co-staining with propidium iodide, which indicates a necrotic cell death mechanism since the presence of an intact plasma membrane would prevent propidium iodide from entering early apoptotic cells.[61] To exclude a photoredox-based MOA[23-24] of **1b** in HeLa cells, the intracellular NAD/NADH levels (**Fig. S17**) and GSH/GSSG levels (**Fig. S18**) of HeLa cells treated with **1b** upon irradiation were determined as described in **S32-S33**. No relevant changes in levels of either NAD/NADH or GSH/GSSG are observed upon treatment with **1b** and subsequent irradiation in the range size of its IC_{50} value. This shows that the MOA of **1b** in HeLa cells is not photoredox-induced.

To investigate the clusters formed by **1a** and **1b** that were observed in the intracellular localization experiments (**Fig. 3**), dynamic light scattering (DLS) was used as described in **S34** to examine whether aggregates of **1a** and **1b** form in the cellular environment (**Tab. S14**). Both **1a** and **1b** form aggregates in DMEM, which was used as a model system to test the aggregation behaviour since it is the most common cell medium for culturing mammalian cells.[62] For **1a** an aggregate size distribution of 122 ± 46 (31.4%), 6 ± 2 (51.3%), and 0.65 ± 0.04 (31.4%) nm was observed, for **1b** a size distribution of 4620 ± 819 (2.0%), 86 ± 33 (79.7%), and 3.8 ± 0.6 (18.3%) nm was observed. Aggregates formed by **1b** in the cell upon irradiation could give rise to a photothermal MOA of **1b** upon irradiation involving a that triggers cell death pathway through the local light-to-heat generation, by the compound clusters similar to nanomaterials applied in PTT.[25] To test this hypothesis, the specific absorption rates (SARs), which are used in literature to experimentally quantify the heating efficiency of compounds[63], of **1a** and **1b** were determined using a lock-in thermal imaging setup (LIT) measuring the corresponding amplitude (**Fig. S19**) as described in **S35**. Compound **1b** shows overall higher SAR values compared to **1a** (**Tab. 4, Fig. 4**), which is in line with the behaviour of the compounds regarding photocytotoxicity (**Tab. 2**). While the SAR values of **1a** lie in a compound concentration range of 6.25 μM to 100 μM virtually steady slightly below 2000 W/g, the ones of **1b** show a clear dependency on the concentration ranging from around 16'000 W/g at 100 μM to 6000 W/g at 6.25μM. This shows the SAR of **1b** increases with lower concentrations, most likely due to the higher solvated state of individual molecules, indicating that at compound concentrations present in HeLa cells a photothermal MOA emerging from locally formed clusters of **1b** is conceivable.

Compound	Concentration (μM)	Amplitude A (K) × 10^{-3}	Heating Slope β (K/s) × 10^{-2}	SAR (W/g) × 10^{3}
1a	6.25	0.1 ± 0.1	0.2 ± 0.2	1.7 ± 1.5
1a	12.5	0.3 ± 0.1	0.4 ± 0.2	1.9 ± 0.8
1a	25	0.54 ± 0.07	0.7 ± 0.1	1.6 ± 0.2
1a	50	1.33 ± 0.06	1.7 ± 0.1	1.97 ± 0.09
1a	100	2.5 ± 0.3	3.1 ± 0.4	1.8 ± 0.2
1b	6.25	1.8 ± 0.2	2.3 ± 0.2	16 ± 1
1b	12.5	3.2 ± 0.2	4.0 ± 0.2	14.0 ± 0.8
1b	25	5.8 ± 0.3	7.3 ± 0.3	12.8 ± 0.6
1b	50	8.7 ± 0.1	10.9 ± 0.1	9.6 ± 0.1
1b	100	11.3 ± 0.4	14.2 ± 0.5	6.2 ± 0.2

Tab. 4. The measured amplitude A, heating slope β, and calculated specific absorption rates (SAR) for **1a** and **1b** based on measurements by lock-in thermal imaging (LIT).

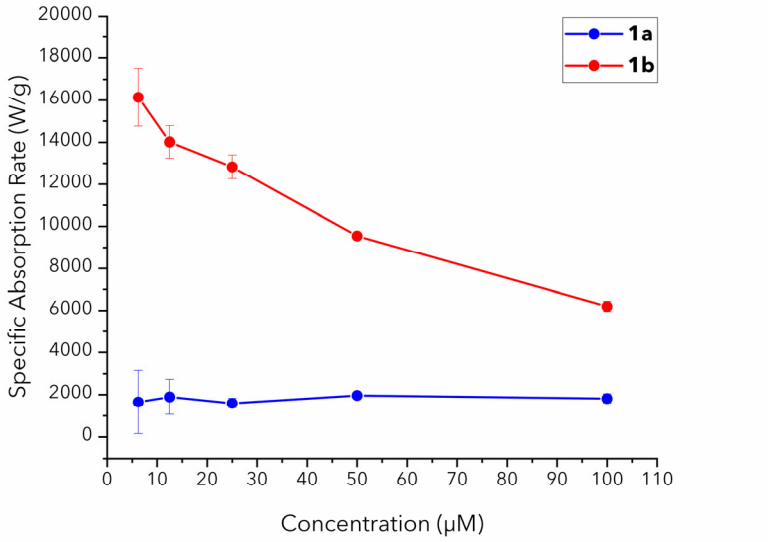

Fig. 4: Specific absorption rates (W/g) of **1a** and **1b** plotted versus the concentration. A clear increase of the SAR values for lower concentrations of **1b** is observed, while the SAR of **1a** virtually shows no concentration dependency.

Discussion:

The presence of molecular oxygen in the tissue to be treated plays a crucial role in the MOA of PDT, making this approach ineffective in tumours surrounded by necrotic tissue or dense tumour masses.[64] Different strategies, such as the application of oxygen vehicles, have been proposed to overcome the barrier posed to PDT by the hypoxic environment in solid tumours.[65] This environment arises from the abnormal structure of the microvessels and tumour microenvironment that leads to ineffective blood distribution,[65] and leads to low

oxygen levels that limit PDT.[66] PTT is one photoinduction strategy that would circumvent this limitation, since the therapeutic efficiency of PTT is not affected by oxygen levels.[67] It is even possible that PDT could be combined with PTT to produce a synergistic effect, even in solid tumours.[67-68]

Here we examined small molecules that can act as photothermal agents. With only minute levels of ROS generated upon irradiation, as detected by applied ROS sensors (**Fig. S6**) in PBS as well as intracellularly in HeLa cells (**Fig. S11-S12**), the main MOA of **1a, 1b, 2a, 2b**, **3a**, and **3b** is photothermal (**Tab. 4, Fig. 4**) and bypasses the limitation of PDT. A particularly interesting insight comes from examination of the compound pair **3a** and **3b**. While both compounds show an energetically accessible first excited triplet state (T_1) energy levels based on the results from TDDFT simulations (**Tab. S7-S8**), no $^1O_2$ production was observed (**Tab. 1**), which is in line with the non-existent T_1 state observed in the τ_T measurements (**Tab. 1**). Despite this, both compounds show high photocytotoxicity (**Tab. 2**).

The oxygen-independent MOA of the most effective compound, **1b**, was demonstrated upon irradiation under hypoxia in HeLa cells (**Tab. S12**), where virtually no change in the high effectivity was observed. Additionally, a high efficiency of **1b** in HeLa MCTS was confirmed upon irradiation (**Fig. 2**), underlining the effectivity of the reported agents. Despite the benefits of the MOA of PTT regarding tumour hypoxia, bio- and nanomaterials applied in PTT show limitations especially concerning biocompatibility, biodegradation and long-term toxicity.[25] Compounds **1a, 1b, 2a, 2b**, **3a**, and **3b** are all small molecules with molecular weights below 600 g/mol, and do not contain any metal atoms. Their non-toxic behaviour in HeLa cells in the dark is indicated by an experimental IC_{50} value up to and > 5 mM. However, upon irradiation these compounds become potent photocytotoxic agents with IC_{50} values as low as 0.0060 ± 0.0003 μM (**Tab. 2**), showing that their molecular character overcomes the biocompatibility problems of materials currently applied in PTT.

Conclusions:

The experiments presented have shown that the reported compounds **1a, 1b, 2a, 2b**, **3a**, and **3b** show multiple advantages over established agents for PDT as well as PTT. The novel compounds are easily accessible synthetically and are all metal-free small molecules. They are virtually non-toxic in the dark, which bypasses the biocompatibility/-degradation and toxicity issues found in the applied materials previously used for PTT. SAR determination experiments demonstrate the light-to-heat generation abilities of these compounds, especially of **1b** which shows particularly high SAR values with low concentrations. The agents are also over 830'000 times more toxic after light activation combined with a photothermal and oxygen-independent MOA (PI of over 360'000 under hypoxic condition of 0.2% O_2), to the best of our knowledge the highest values reported so far (compare with [69]). In short, these compounds show high potential for overcoming the existing drawbacks of PDT and PTT.

Acknowledgements:

We thank the University of Zurich and the R'Equip programme of the Swiss National Science Foundation (project number 206021_164018) for financial support. L.S. was supported by a UZH Forschungskredit grant (Forschungskredit-Beitrag FK-085-19, co-financed together with the Colbianco Stiftung). We kindly thank Prof. Dr. Roland H. Wenger for providing us with

the hypoxia facility and Patrick Spielmann for his help in carrying out the hypoxia experiments. We thank Dr. Thomas Fox for assistance with NMR spectroscopy, Dr. Frank Schumer for synthesizing the APF, Dr. Sabbi Lall from Life Science Editors for valuable comments about our manuscript and PD Dr. Stefano Ferrari as well as Prof. Dr. Pablo Rivera-Fuentes for stimulating discussions. Imaging was performed with support and equipment maintained by the Center for Microscopy and Image Analysis, University of Zurich. FACS experiments were performed with support and equipment maintained by the Cytometry Facility, University of Zurich. The authors would like to acknowledge the company NanoLockin for providing the Calorsito device.

Competing Interests:

M. B. has an equity interest in the company NanoLockin GmbH, that may potentially benefit from the research results.

Data Availability:

Unless mentioned otherwise in the corresponding section, the data that support the findings of this study are available within the paper and its Supplementary Information, or from the corresponding authors on reasonable request. CCDC 2108866–2108875 contain the supplementary crystallographic data for this paper. These data are provided free of charge by The Cambridge Crystallographic Data Centre via www.ccdc.cam.ac.uk/structures.

References:

1 J. Zhang, C. Jiang, J. P. Figueiró Longo, R. B. Azevedo, H. Zhang and L. A. Muehlmann, *Acta Pharm. Sin. B*, 2018, **8**, 137-146.
2 M. Lan, S. Zhao, W. Liu, C.-S. Lee, W. Zhang and P. Wang, *Adv. Healthcare Mater.*, 2019, **8**, 1900132.
3 P. De Silva, M. A. Saad, H. C. Thomsen, S. Bano, S. Ashraf and T. Hasan, *J. Porphyrins Phthalocyanines*, 2020, **24**, 1320-1360.
4 D. van Straten, V. Mashayekhi, H. S. de Bruijn, S. Oliveira and D. J. Robinson, *Cancers*, 2017, **9**, 19.
5 P. Agostinis, K. Berg, K. A. Cengel, T. H. Foster, A. W. Girotti, S. O. Gollnick, S. M. Hahn, M. R. Hamblin, A. Juzeniene, D. Kessel, M. Korbelik, J. Moan, P. Mroz, D. Nowis, J. Piette, B. C. Wilson and J. Golab, *CA Cancer J. Clin.*, 2011, **61**, 250-281.
6 R. L. Yanovsky, D. W. Bartenstein, G. S. Rogers, S. J. Isakoff and S. T. Chen, *Photodermatol. Photoimmunol. Photomed.*, 2019, **35**, 295-303.
7 H. Abrahamse and M. R. Hamblin, *Biochem. J.*, 2016, **473**, 347-364.
8 T. S. Herman, B. A. Teicher and L. S. Collins, *Cancer Res.*, 1988, **48**, 2342-2347.
9 J. M. Brown, *Methods Enzymol.*, 2007, **435**, 295-321.
10 M. S. Baptista, J. Cadet, P. Di Mascio, A. A. Ghogare, A. Greer, M. R. Hamblin, C. Lorente, S. C. Nunez, M. S. Ribeiro, A. H. Thomas, M. Vignoni and T. M. Yoshimura, *Photochem. Photobiol.*, 2017, **93**, 912-919.
11 B. Pucelik, A. Sułek, A. Barzowska and J. M. Dąbrowski, *Cancer Lett.*, 2020, **492**, 116–135.
12 L. Hong, J. Li, Y. Luo, T. Guo, C. Zhang, S. Ou, Y. Long and Z. Hu, *Biomolecules*, 2022, **12**, 81.
13 B. C. Wilson and M. S. Patterson, *Phys. Med. Biol.*, 2008, **53**, R61-R109.
14 D. Gál, *Biochem. Biophys. Res. Commun.*, 1992, **186**, 1032-1036.
15 T. Vidóczy, S. Elzemzam and D. Gál, *Biochem. Biophys. Res. Commun.*, 1992, **189**, 1548-1552.

16 T. Kriska, J. Jakus, A. Keszler, R. Vanyur, A. Nemeth and D. Gal, *Proc. SPIE*, 1999, **3563**, 11-17.
17 D. Gal, T. Kriska, T. Shutova and A. Nemeth, *Proc. SPIE*, 2001, **4248**, 169-178.
18 K. M. Scherer, R. H. Bisby, S. W. Botchway and A. W. Parker, *Anti-Cancer Agents Med. Chem.*, 2017, **17**, 171-189.
19 I. Yoon, J. Z. Li and Y. K. Shim, *Clin. Endosc.*, 2013, **46**, 7-23.
20 G. Smith, W. G. McGimpsey, M. C. Lynch, I. E. Kochevar and R. W. Redmond, *Photochemistry and Photobiology*, 1994, **59**, 135-139.
21 F. Dall'Acqua and P. Martelli, *J. Photochem. Photobiol. B*, 1991, **8**, 235-254.
22 M. R. Hamblin and H. Abrahamse, *Antibiotics*, 2020, **9**, 53.
23 H. Y. Huang, S. Banerjee, K. Q. Qiu, P. Y. Zhang, O. Blacque, T. Malcomson, M. J. Paterson, G. J. Clarkson, M. Staniforth, V. G. Stavros, G. Gasser, H. Chao and P. J. Sadler, *Nat. Chem.*, 2019, **11**, 1041-1048.
24 M. Li, K. H. Gebremedhin, D. Ma, Z. Pu, T. Xiong, Y. Xu, J. S. Kim and X. Peng, *J. Am. Chem. Soc.*, 2022, **144**, 163-173.
25 W. Wei, X. Zhang, S. Zhang, G. Wei and Z. Su, *Mater. Sci. Eng. C*, 2019, **104**, 109891.
26 H. S. Jung, P. Verwilst, A. Sharma, J. Shin, J. L. Sessler and J. S. Kim, *Chem. Soc. Rev.*, 2018, **47**, 2280-2297.
27 S. Anand, T. A. Chan, T. Hasan and E. V. Maytin, *Pharmaceuticals*, 2021, **14**, 447.
28 Z. He, L. Zhao, Q. Zhang, M. Chang, C. Li, H. Zhang, Y. Lu and Y. Chen, *Adv. Funct. Mater.*, 2020, **30**, 1910301.
29 X. Li, F. Fang, B. Sun, C. Yin, J. Tan, Y. Wan, J. Zhang, P. Sun, Q. Fan, P. Wang, S. Li and C.-S. Lee, *Nanoscale Horiz.*, 2021, **6**, 177-185.
30 S. Huang, R. K. Kannadorai, Y. Chen, Q. Liu and M. Wang, *Chem. Commun.*, 2015, **51**, 4223-4226.
31 A. Naik, R. Rubbiani, G. Gasser and B. Spingler, *Angew. Chem. Int. Ed.*, 2014, **53**, 6938-6941.
32 P. M. Antoni, A. Naik, I. Albert, R. Rubbiani, S. Gupta, P. Ruiz-Sanchez, P. Munikorn, J. M. Mateos, V. Luginbuehl, P. Thamyongkit, U. Ziegler, G. Gasser, G. Jeschke and B. Spingler, *Chem. Eur. J.*, 2015, **21**, 1179-1183.
33 E. Hao, Y. Xu, C. Yu and L. Jiao, CN103952001B, 2014.
34 R. Padrutt, V. Babu, S. Klingler, M. Kalt, F. Schumer, M. I. Anania, L. Schneider and B. Spingler, *ChemMedChem*, 2021, **16**, 694-701.
35 Y.-F. Xiao, J.-X. Chen, W.-C. Chen, X. Zheng, C. Cao, J. Tan, X. Cui, Z. Yuan, S. Ji, G. Lu, W. Liu, P. Wang, S. Li and C.-S. Lee, *Chem. Commun.*, 2021, **57**, 4902-4905.
36 X.-J. Jiang, J. T. F. Lau, Q. Wang, D. K. P. Ng and P.-C. Lo, *Chem. Eur. J.*, 2016, **22**, 8273-8281.
37 L. Schneider, M. Larocca, W. Wu, V. Babu, R. Padrutt, E. Slyshkina, C. König, S. Ferrari and B. Spingler, *Photochem. Photobiol. Sci.*, 2019, **18**, 2792-2803.
38 R. Rubbiani, W. Wu, A. Naik, M. Larocca, L. Schneider, R. Padrutt, V. Babu, C. König, D. Hinger, C. Maake, S. Ferrari, G. Gasser and B. Spingler, *Chem. Commun.*, 2020, **56**, 14373-14376.
39 N. A. Le, V. Babu, M. Kalt, L. Schneider, F. Schumer and B. Spingler, *J. Med. Chem.*, 2021, **64**, 6792–6801.
40 L. Schneider, M. Kalt, M. Larocca, V. Babu and B. Spingler, *Inorg. Chem.*, 2021, **60**, 9416–9426.
41 K. Rurack, M. Kollmannsberger and J. Daub, *Angew. Chem. Int. Ed.*, 2001, **40**, 385-387.
42 M. Baruah, W. Qin, C. Flors, J. Hofkens, R. A. L. Vallée, D. Beljonne, M. Van der Auweraer, W. M. De Borggraeve and N. Boens, *J. Phys. Chem. A*, 2006, **110**, 5998-6009.
43 E. Deniz, G. C. Isbasar, Ö. A. Bozdemir, L. T. Yildirim, A. Siemiarczuk and E. U. Akkaya, *Org. Lett.*, 2008, **10**, 3401-3403.
44 B. Pucelik, R. Paczynski, G. Dubin, M. M. Pereira, L. G. Arnaut and J. M. Dabrowski, *PLoS One*, 2017, **12**, e0185984.
45 A. D. Becke, *Phys. Rev. A*, 1988, **38**, 3098-3100.
46 C. Lee, W. Yang and R. G. Parr, *Phys. Rev. B*, 1988, **37**, 785-789.
47 A. D. Becke, *J. Chem. Phys.*, 1993, **98**, 5648-5652.

48 P. J. Stephens, F. J. Devlin, C. F. Chabalowski and M. J. Frisch, *J. Chem. Phys.*, 1994, **98**, 11623-11627.
49 R. L. Martin, *J. Chem. Phys.*, 2003, **118**, 4775-4777.
50 A. Klamt and G. Schüürmann, *J. Chem. Soc., Perkin Trans. 2*, 1993, 799-805.
51 J. Karges, S. Kuang, F. Maschietto, O. Blacque, I. Ciofini, H. Chao and G. Gasser, *Nat. Commun.*, 2020, **11**, 3262.
52 J. Friedrich, C. Seidel, R. Ebner and L. A. Kunz-Schughart, *Nat. Prot.*, 2009, **4**, 309-324.
53 B. Muz, P. de la Puente, F. Azab and A. K. Azab, *Hypoxia*, 2015, **3**, 83-92.
54 C. Li, M. Yu, Y. Sun, Y. Wu, C. Huang and F. Li, *J. Am. Chem. Soc.*, 2011, **133**, 11231-11239.
55 R. M. Lazarenko, C. E. DelBove, C. E. Strothman and Q. Zhang, *Sci. Rep.*, 2017, **7**, 5061.
56 J. N. Harper and S. H. Wright, *Amer. J. Physiol. Renal Phys.*, 2012, **304**, F56-F67.
57 J.-E. Ricci, C. Muñoz-Pinedo, P. Fitzgerald, B. Bailly-Maitre, G. A. Perkins, N. Yadava, I. E. Scheffler, M. H. Ellisman and D. R. Green, *Cell*, 2004, **117**, 773-786.
58 V. P. Skulachev, *Apoptosis*, 2006, **11**, 473-485.
59 I. Vermes, C. Haanen, H. Steffens-Nakken and C. Reutellingsperger, *J. Immunol. Methods*, 1995, **184**, 39-51.
60 I. Vermes, C. Haanen and C. Reutelingsperger, *J. Immunol. Methods*, 2000, **243**, 167-190.
61 Z. Darzynkiewicz, S. Bruno, G. Del Bino, W. Gorczyca, M. A. Hotz, P. Lassota and F. Traganos, *Cytometry*, 1992, **13**, 795-808.
62 S. R. Hemelaar, A. Nagl, F. Bigot, M. M. Rodríguez-García, M. P. de Vries, M. Chipaux and R. Schirhagl, *Microchim. Acta*, 2017, **184**, 1001-1009.
63 L. Steinmetz, C. Kirsch, C. Geers, A. Petri-Fink and M. Bonmarin, *Nanomaterials*, 2020, **10**, 1665.
64 G. M. F. Calixto, J. Bernegossi, L. M. de Freitas, C. R. Fontana and M. Chorilli, *Molecules*, 2016, **21**, 342.
65 L. Larue, B. Myrzakhmetov, A. Ben-Mihoub, A. Moussaron, N. Thomas, P. Arnoux, F. Baros, R. Vanderesse, S. Acherar and C. Frochot, *Pharmaceuticals*, 2019, **12**, 163.
66 G. Gunaydin, M. E. Gedik and S. Ayan, *Front. Chem.*, 2021, **9**, 691697.
67 W. Bian, Y. Wang, Z. Pan, N. Chen, X. Li, W.-L. Wong, X. Liu, Y. He, K. Zhang and Y.-J. Lu, *ACS Appl. Nano Mater.*, 2021, **4**, 11353-11385.
68 B. Tian, C. Wang, S. Zhang, L. Feng and Z. Liu, *ACS Nano*, 2011, **5**, 7000-7009.
69 H. D. Cole, J. A. Roque, G. Shi, L. M. Lifshits, E. Ramasamy, P. C. Barrett, R. O. Hodges, C. G. Cameron and S. A. McFarland, *J. Am. Chem. Soc.*, 2022, **144**, 9543–9547.